PERGAMON

International Journal of Heat and Mass Transfer 45 (2002) 5171–5190

International Journal of HEAT and MASS TRANSFER

www.elsevier.com/locate/ijhmt

Mixed convection heat transfer in two-dimensional open-ended enclosures

Khalil Khanafer [a], Kambiz Vafai [b,*], Marilyn Lightstone [a]

[a] *Mechanical Engineering Department, McMaster University, Hamilton, Canada L8S 4L7*
[b] *Mechanical Engineering Department, University of California, Riverside, CA 92521, USA*

Received 27 April 2002; received in revised form 7 June 2002

Abstract

Mixed convection heat transfer in open-ended enclosures has been studied numerically for three different flow angles of attack. Discretization of the governing equations is achieved using a finite element scheme based on the Galerkin method of weighted residuals. Comparisons with previously published work on special cases of the problem are performed and the results show excellent agreement. A wide range of pertinent parameters such as Grashof number, Reynolds number, and the aspect ratio are considered in the present study. The obtained results show that thermal insulation of the cavity can be achieved through the use of high horizontal velocity flow. Various results for the streamlines, isotherms and the heat transfer rates in terms of the average Nusselt number are presented and discussed for different parametric values.

Keywords: Mixed convection; Open-ended cavity; Extended domain

1. Introduction

Buoyancy-driven flow and heat transfer in open-ended enclosures is receiving increasing attention by many researchers in recent years. Natural convection in open-ended cavities has been the subject of interest both experimentally and numerically. This is primarily because several applications of practical interest, such as nuclear reactors, fire research, thermal insulation, thermal storage systems, electric transmission cables, and brake housing of an aircraft [1], can be modeled by various extensions of this type of geometry.

Penot [2] conducted numerical computations of two-dimensional free convection flow inside an isothermal open square cavity. The governing equations were solved in an enlarged computational domain by utilizing the far-field boundary conditions and the effect of inclination and Grashof number were examined. His results indicated the existence of unsteady solutions for a vertical cavity for Grashof numbers higher than 10^5. LeQuere et al. [3] considered a numerical calculation of thermally driven two-dimensional unsteady laminar flow in cavities of rectangular cross section using primitive variables. The results of this investigation showed that the overall heat transfer rates from the cavity increase with an increase in the values of Grashof numbers and aspect ratios.

Chan and Tien [4] performed a numerical study of two-dimensional laminar natural convection in a square open cavity with a heated vertical wall and two insulated horizontal walls for Rayleigh numbers ranging from 10^3 to 10^9. Calculations were made in an extended computational domain beyond the aperture plane for a Prandtl number of 1. The obtained heat transfer results were found to approach those of natural convection over a vertical isothermal flat plate. Later on, the same authors [5] studied laminar, steady-state natural convection in a two-dimensional shallow rectangular open enclosure for Rayleigh number up to 10^6. The computational domain was restricted to the cavity region and approximate boundary conditions were applied directly at the

* Corresponding author. Tel.: +1-909-787-2135; fax: +1-909-787-2899.
E-mail address: vafai@engr.ucr.edu (K. Vafai).

0017-9310/02/$ - see front matter
PII: S0017-9310(02)00219-3

Nomenclature

AR	aspect ratio of the enclosure (AR $= w/H$)
H	height of the enclosure, m
L_x	extended computational domain length in x-direction, m
L_y	extended computational domain length in y-direction, m
n	outward normal to a surface
Nu	Nusselt number
p	pressure, Pa
P	dimensionless pressure
Pr	Prandtl number (v/α)
Ra	Rayleigh number ($(g\beta H^3\Delta T)/(v\alpha)$)
Re	Reynolds number (HU_0/v)
Ri	Richardson number (Gr/Re^2)
T	temperature, °C
T_w	enclosure wall temperature, °C
θ	dimensionless temperature
u	velocity in the x-direction, m s^{-1}
v	velocity in the y-direction, m s^{-1}
U_o	external flow velocity, m s^{-1}
U	dimensionless velocity in the x-direction
V	dimensionless velocity in the y-direction
w	width of the enclosure, m
x, y	cartesian coordinates, m

Greek symbols

α	thermal diffusivity, m^2 s^{-1}
β	coefficient of volume expansion, K^{-1}
ϕ	inclination angle
μ	dynamic viscosity, kg m^{-1} s^{-1}
v	kinematic viscosity, m^2 s^{-1}
ρ	density, kg m^{-3}

Subscripts

∞	condition at infinity
w	wall of the enclosure

aperture plane using constant properties and Boussinesq approximation. This approach did not predict some of the important features of the flow field near the aperture plane of the cavity since the corner and outer region were not included in the analysis. Other studies involving two-dimensional natural convection in open enclosures were studied by Doria [6] for predicting fire spread in a room and by Jacobs et al. [7,8] in modeling circulation above city streets and geothermal reservoirs.

Experimental studies for natural convection in open cavities were illustrated by Humphrey and co-workers [9] and Sernas and Kyriakides [10] in modeling solar systems. Showole and Tarasuk [11] conducted experimental and numerical studies of natural convection with flow separation in upward-facing inclined open cavities for Prandtl number of 0.7 and Rayleigh number from 10^4 to 5×10^5 and a wide range of aspect ratios and inclination angles. The results of this investigation showed that the average heat transfer increased significantly for all Rayleigh numbers for the case of upward facing cavity. Elsayed and Chakroun [12] performed an experimental study for steady-state natural convection from a square, tilted partially open cavity for different geometrical arrangements of the opening. The results showed that the heat transfer coefficient was independent of the geometrical arrangement of the opening for tilt angles between 75° and 90°. In addition, the heat transfer coefficient was found to increase sharply with decreasing tilt angle until an angle of 0° was reached.

A broad study was conducted by Vafai and Ettefagh [13] for investigating basic aspects and physics of the flow field within the open-ended structures and the effect of extended computational domain on flow and heat transfer inside the open-ended cavity and its immediate surroundings. They illustrated in this study that the required extent of the enlarged computational domain for obtaining accurate results was much larger than that shown by previous investigators. In addition, they showed that the far field flow characteristics were sensitive to the type of boundary conditions used. Their study also included the effect of the Rayleigh number, Prandtl number, temperature ratio (between the upper and lower blocks), and the aspect ratio of the cavity. The thermal and fluid flow instabilities in natural convection in open-ended cavities were also analyzed for the first time by Vafai and Ettefagh [14]. They showed, at higher Rayleigh numbers, the existence of periodic oscillations in the Nusselt number corresponds to the central vortex's oscillations and its location inside the cavity. The frequency of these oscillations was found to increase linearly with Rayleigh number.

Mhiri et al. [15] performed a numerical study of laminar mixed convection in a cavity with a vertical downstream air jet. The numerical results showed that the entries and the exits of the fluid in the cavity could efficiently be avoided by operating with high air flow rates. Later on, the same authors [16] conducted a numerical study of the thermal insulation of a heated two-dimensional cavity limited on its superior part by a horizontal plane air jet. A finite difference method was developed in this investigation to solve the dimensionless governing equations for Reynolds number of 50 and 500. The obtained results showed that the heat exchange between the interior of the cavity and the surrounding

medium could be avoided when operating with high velocities of ejection of the air jet.

The extension of the open-ended domain requires substantially larger memory and computational time. An appropriate set of effective boundary conditions at the aperture plane of the open-ended structure will drastically reduce the storage capacity and the CPU of the computer resources. Recently, Khanafer and Vafai [17,18] performed comprehensive studies for the elimination of the extended boundaries in open-ended structures for both two and three-dimensional geometries. An accurate set of effective boundary conditions for both the flow and the temperature fields was obtained covering a wide range of controlling parameters such as Raleigh number, Prandtl number, and aspect ratios for a partially open-ended geometry. The authors in these investigations showed that the use of the effective boundary conditions resulted in substantial savings in CPU and memory usage.

To the best knowledge of the authors, no attention has been paid to the problem of mixed convection in open-ended enclosures. The present work focuses on conducting a comprehensive study on the effect of different flow configurations on mixed convection heat transfer in open-ended enclosures for a wide range of pertinent controlling parameters. These parameters include the Reynolds number *Re*, Grashof number *Gr*, and aspect ratio AR.

2. Physical model and assumptions

A two-dimensional cavity of height H and width $2w$ is considered in the present investigation as shown in Fig. 1a. Due to the symmetry consideration, half of the open-ended cavity is used in the present study as shown in Fig. 1b. The validity of using the symmetry conditions at the centerline of the cavity was checked thoroughly through a series of numerical runs. The horizontal walls are maintained at a constant temperature T_w, while the surrounding fluid interacting with the open-ended enclosure is at an ambient temperature T_∞, which is lower than T_w. The walls at the proximity of the aperture plane of the cavity are assumed to be adiabatic. The working fluid is Newtonian, and the flow is assumed laminar and incompressible. The fluid properties are assumed constant

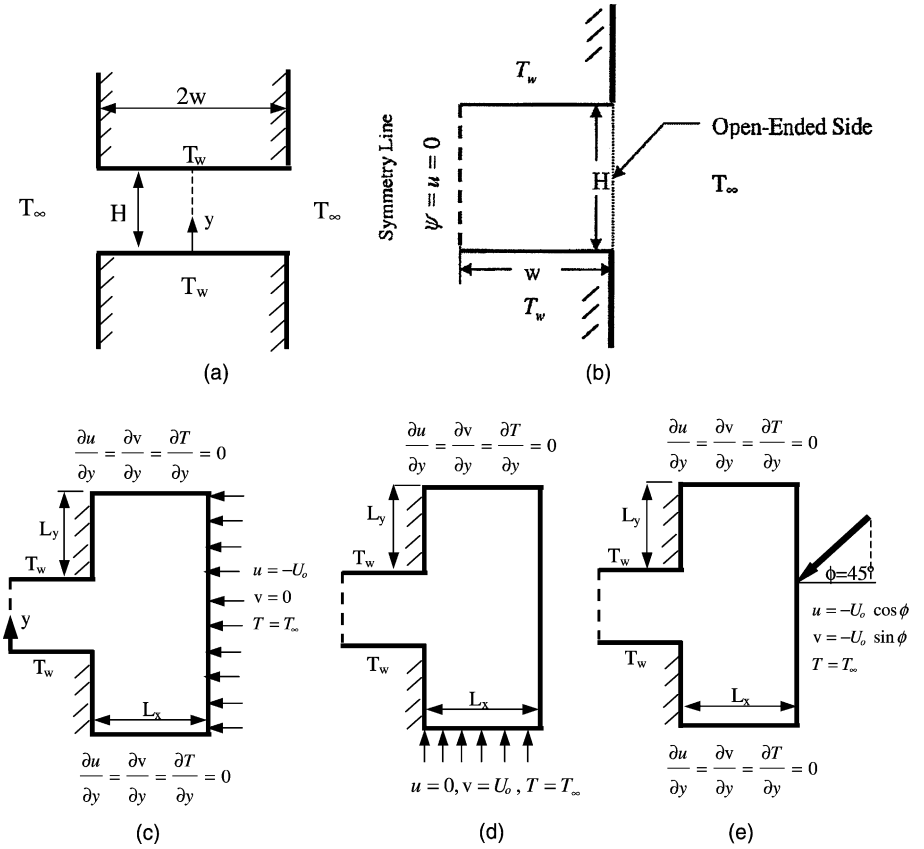

Fig. 1. (a) Physical domain, (b) physical domain utilizing the symmetry condition, (c) horizontal flow, (d) vertical flow, and (e) inclined flow.

except for the density ρ, which is assumed to vary linearly with temperature according to the Boussinesq approximation. Furthermore, viscous dissipation and Joule heating are assumed negligible in the present study. The working fluid was assumed to be air ($Pr = 0.7$).

Taking into account the above mentioned assumptions, the governing equations can be written in non-dimensional form as follows:

$$\nabla \cdot \mathbf{V} = 0 \tag{1}$$

$$\frac{\partial \mathbf{V}}{\partial \tau} + (\mathbf{V} \cdot \nabla)\mathbf{V} = \frac{1}{Re}\nabla^2 \mathbf{V} + \frac{Gr}{Re^2}\theta - \nabla P \tag{2}$$

$$\frac{\partial \theta}{\partial \tau} + \mathbf{V} \cdot \nabla \theta = \frac{1}{Pr\,Re}\nabla^2 \theta \tag{3}$$

where $Re = (U_o H)/v$ is the Reynolds number, $Gr = (g\beta_T \Delta T H^3)/v^2$ is the thermal Grashof number, and $Pr = v/\alpha$ is the Prandtl number. The aspect ratio AR is defined as $\mathrm{AR} = w/H$.

Eqs. (1)–(3) were cast in non-dimensional form by using the following:

$$(X, Y) = \frac{(x, y)}{H}, \quad (U, V) = \frac{(u, v)}{U_o}, \quad \theta = \frac{T - T_\infty}{T_w - T_\infty}, \quad P = \frac{pH}{\mu U_o} \tag{4}$$

2.1. Boundary conditions

The boundary conditions on the extended computational domain for three basic configurations are shown in Fig. 1c–e. The open boundary conditions were approximated by specifying zero normal gradients for the velocities and temperature at these locations. The above approximations resulted in an accurate description of the flow field inside the cavity provided that the computational domain is extended far enough.

2.2. Heat transfer calculations

The heat transfer calculations within the open-ended cavity is measured in terms of the average Nusselt number at the lower and upper walls as follows:

$$\overline{Nu} = \mathrm{AR}\int_0^{\mathrm{AR}} \frac{\partial \theta}{\partial Y}\,\mathrm{d}x \tag{5}$$

2.3. Numerical scheme

The numerical procedure used to solve the governing equations for the present work is based on the Galerkin weighted residual method of finite-element formulation. The application of this technique is well documented [19]. The segregated solution method was chosen to solve the governing equations. The advantage of using this method is that the global system matrix is decomposed into smaller submatrices and then solved in a sequential manner. This approach will result in substantially less storage. A non-uniform grid distribution is implemented in the present investigation especially near the walls to capture the rapid changes in the dependent variable. To test and assess grid independence of the present solution scheme, many numerical runs were performed for higher Grashof and Reynolds numbers as shown in Fig. 2. These experiments revealed that a non-uniform spaced grid of 41×41 for the C-shape cavity is adequate to describe correctly the flow and heat and mass transfer processes inside the cavity. Further increase in the number of grid points produced essentially the same results. The present numerical approach was verified against the published results by Vafai and Ettefagh [13] for natural convection heat transfer in open-ended enclosures for Rayleigh number $Ra = 10^5$ as shown in Fig. 3. It is seen in this comparison that both solutions are in excellent agreement.

3. Results and discussion

A wide range of pertinent parameters such as Reynolds number, Grashof number, and aspect ratio of the enclosure are analyzed in this study. These ranges are varied as $10^2 \leqslant Re \leqslant 10^4$, $10^2 \leqslant Gr \leqslant 10^5$, and $0.25 \leqslant \mathrm{AR} \leqslant 1$.

The effect of Grashof number on the streamlines and the isotherms for different flow configurations is shown in Figs. 4 and 5. It can be seen in Fig. 4 that as the Grashof number increases ($Gr = 10^3$) the temperature of the fluid inside the cavity increases and as a result the hot fluid rises like a buoyant plume into the outside domain. This action is referred to as the ejection mechanism [13,14] caused by the convection heat transfer interaction within the cavity. Therefore, the cold air from the surrounding region creeps in at a faster rate into the lower part of the open enclosure, which is part of the external flow into the cavity, to replace the departing hot fluid. This suction mechanism is responsible for an almost parallel flow along the lower wall of the open cavity. For a higher Grashof number of 10^4, the cold fluid penetrates further inside the open cavity and departs from the upper hot wall at higher speeds as depicted from the closer spaced streamlines at the exit. As the Grashof number increases further (10^5), the cold fluid penetrates into the cavity at much higher velocity. As such, the outgoing fluid rises up at much faster speeds resulting in a thinner wall plume. Fig. 4 shows that the cold fluid penetrates into the cavity at a higher rate for 45° flow angle of attack than other flow configurations. This is because 45° flow angle of attack allows more fluid to penetrate into the cavity ($Gr = 10^4$). In this case, the cold fluid will be sucked into the cavity

at a higher rate for dominant natural convection mechanism than the case for dominant forced convection. For 90° flow angle of attack, the flow field pattern within the enclosure is strongly affected by the Grashof number. For small Grashof number, the main bulk flow does not penetrate much into the cavity due to the predominant effect of the external flow.

Fig. 5 shows the effect of the Grashof number on the isotherms structure within the cavity for Reynolds number of $Re = 100$. It is seen in this figure, ($Gr = 10^3$),

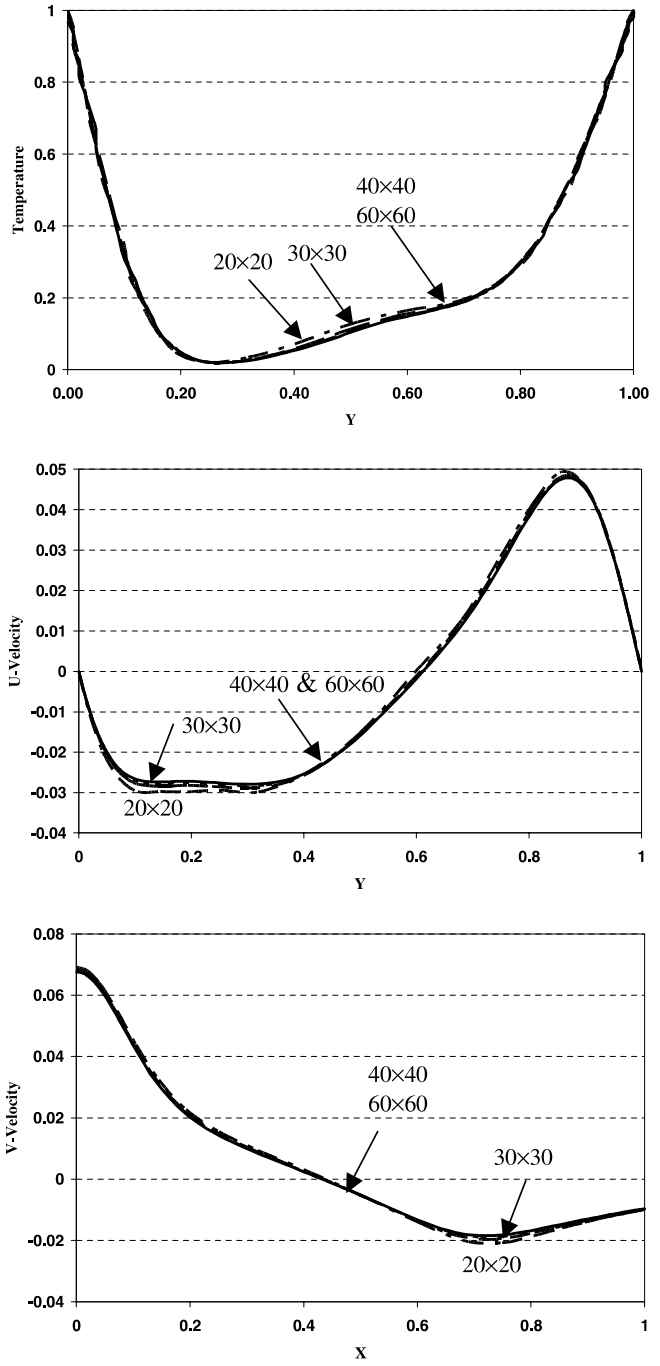

Fig. 2. Effect of the grid size on the temperature and velocity profiles at the mid-sections of the cavity for zero flow angle of attack (AR = 1, $Gr = 10^5$ and $Re = 2500$).

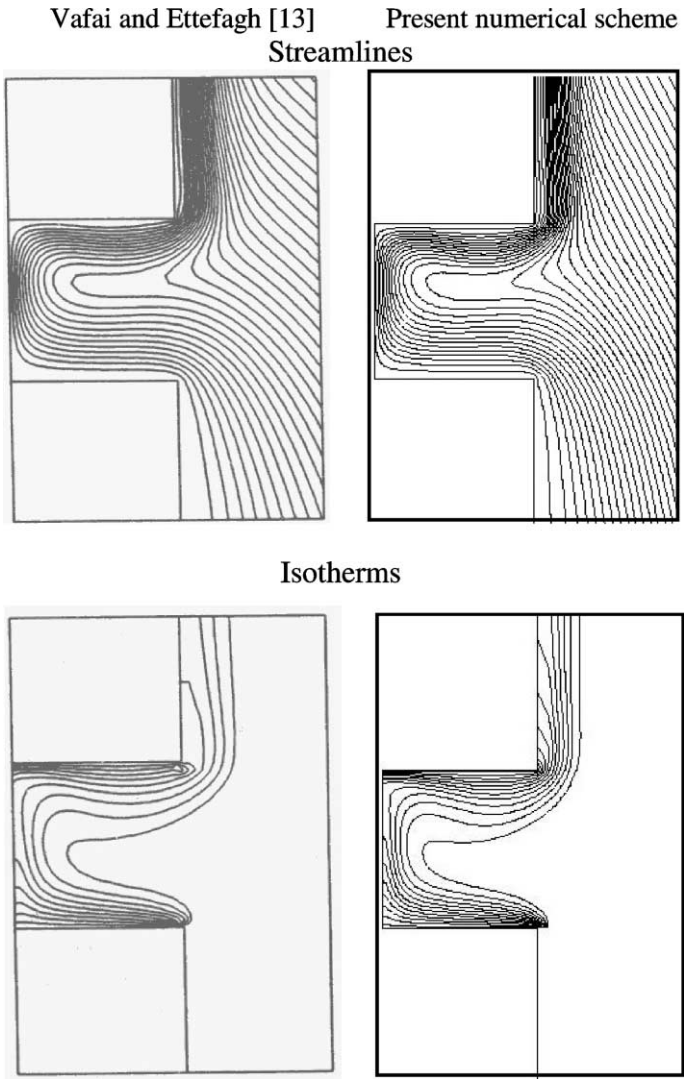

Fig. 3. Comparison of the streamlines and isotherms between the two-dimensional model utilizing the extended boundaries and that of Vafai and Ettefagh [13] for Rayleigh number $Ra = 10^5$.

that heat transfer mechanism inside the cavity is mainly by conduction. As the Grashof number increases, the intensity of convection heat transfer with the cavity increases and the isotherms become closely spaced together along the two horizontal hot walls indicating steep temperature gradients in the vertical direction. The thickness of this thermal layer decreases with an increase in the Grashof number as seen in Fig. 5 ($Gr = 10^5$) and consequently increases the effectiveness of the heat transfer within the cavity as well as with the far field fluid.

Fig. 6 illustrates the influence of an increase in the Reynolds number of the external flow on the flow patterns within the cavity for low Grashof number of 10^2 and aspect ratio of unity. For 0° flow angle of attack, the flow patterns resemble the ones for the case with jet impinging flow on a vertical plate. The flow patterns show symmetry about the horizontal line of the cavity for all values of the Reynolds number. For 45° flow angle of attack, the flow penetrates into the cavity for higher Reynolds number filling the entire cavity with a weak single clockwise central vortex. For high Reynolds number, the flow field is mainly controlled by the external flow. For 90° flow angle of attack, as the Reynolds number increases the speed of the counter clockwise vortex within the cavity increases. As seen in this figure, for three cases, the flow does not penetrate much into the cavity for low Grashof number and high Reynolds number due to the predominant effect of the external flow.

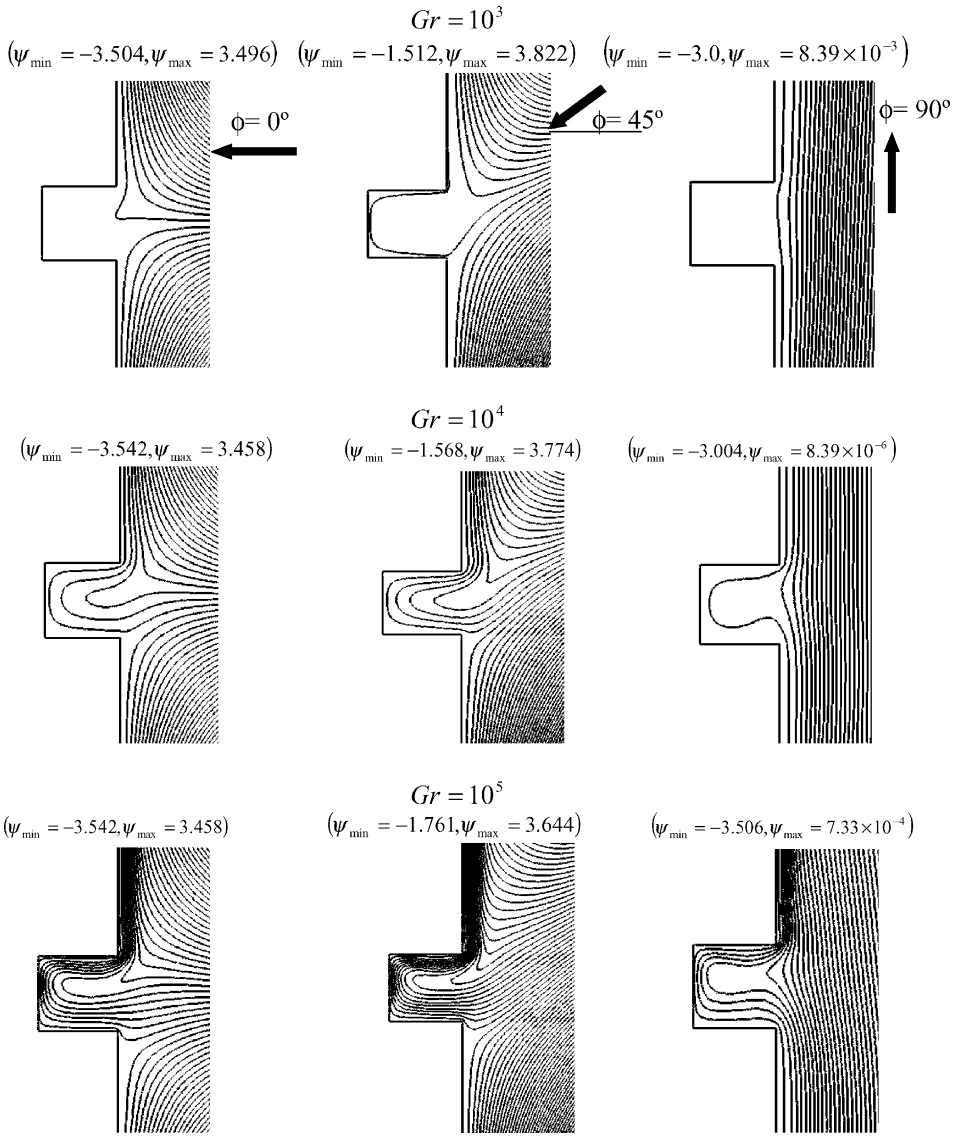

Fig. 4. The effect of Grashof number on the streamlines for three different flow configurations (AR = 1, $Re = 100$).

The effect of an increase in the Reynolds number on the isotherms for different flow configurations at Grashof number of 10^2 and aspect ratio of unity is shown in Fig. 7. Fig. 7 shows a symmetrical behavior of the isotherms about the horizontal centerline of the cavity for 0° flow angle of attack. Due to the symmetry in the isotherms, the heat transfer from the lower and the upper horizontal walls are almost identical. For 45° and 90° flow angle of attacks, the scenario is different in Fig. 7. For 45° flow angle of attack, there exists symmetry in the isotherms for low Reynolds number. As the Reynolds number increases, the symmetry breaks down due to a substantially stronger external flow compared with that of natural convection flow within the cavity. For higher Reynolds numbers, the thermal boundary layer develops along the lower horizontal surface of the cavity and the temperature gradients in the upper part of the cavity decreases, resulting in a thermally-stratified flow along the upper horizontal wall. For 90° flow angle of attack, the isotherm pattern within the cavity changes substantially for high Reynolds number. The isotherms for this case resemble the ones for thermally-driven cavity with moving fluid along the aperture plane. As a result, the isotherms are clustered at the aperture plane due to a high-speed external flow passing over the open cavity. The high-speed counter clockwise vortex within the cavity enhances the heat transfer from the upper horizontal wall. The isotherms at the lower surface are

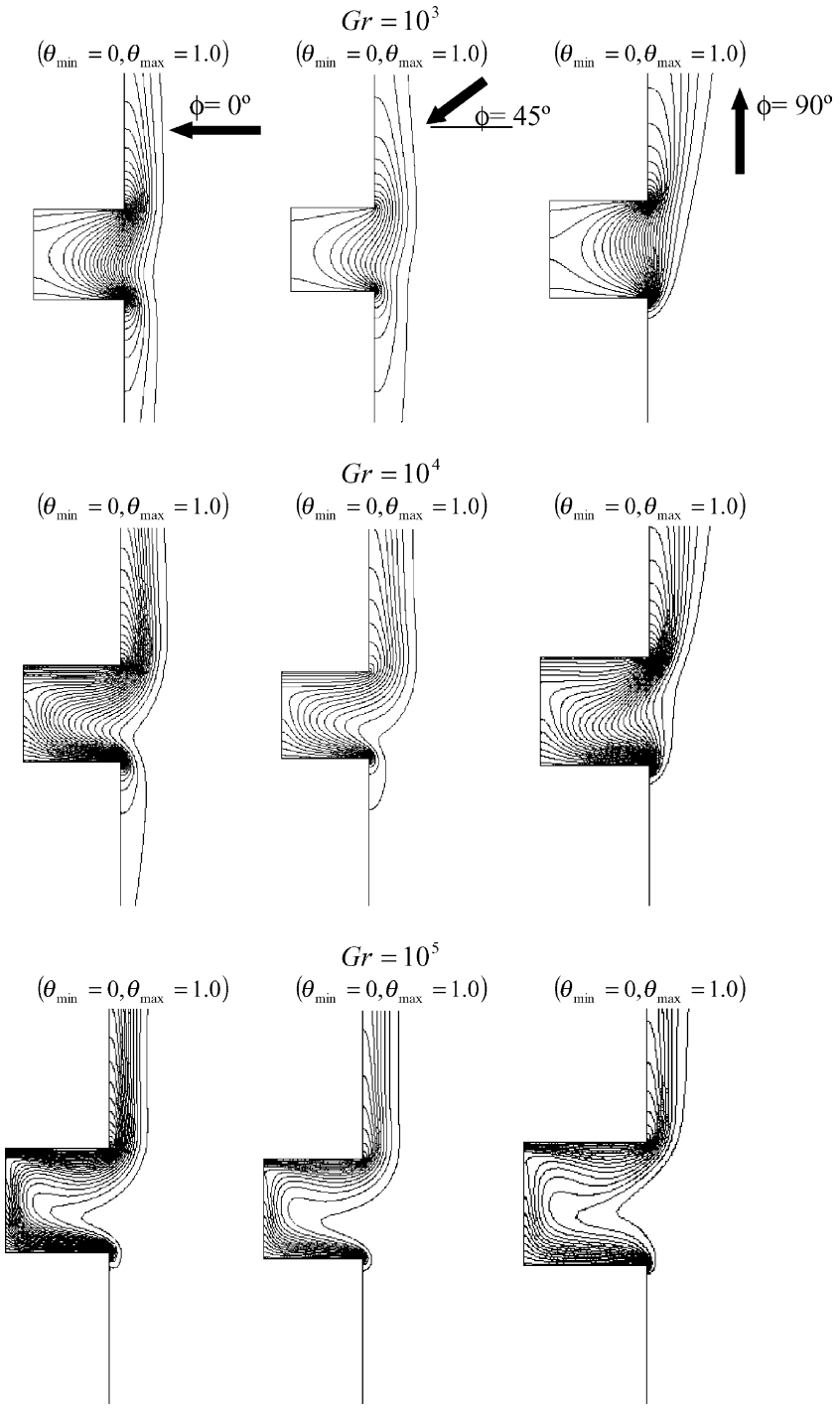

Fig. 5. The effect of Grashof number on the isotherms for three different flow configurations (AR = 1, $Re = 100$).

almost horizontal indicating that most of the heat transfer from this surface is carried out by conduction.

For high Grashof number ($Gr = 10^5$), Fig. 8 shows the effect of varying the Reynolds number on the streamlines and the isotherms for 0° flow angle of attack. As the Reynolds number increases, the flow penetration into the cavity is diminished as a result of strong influence of the external flow. As such, a thinner wall plume

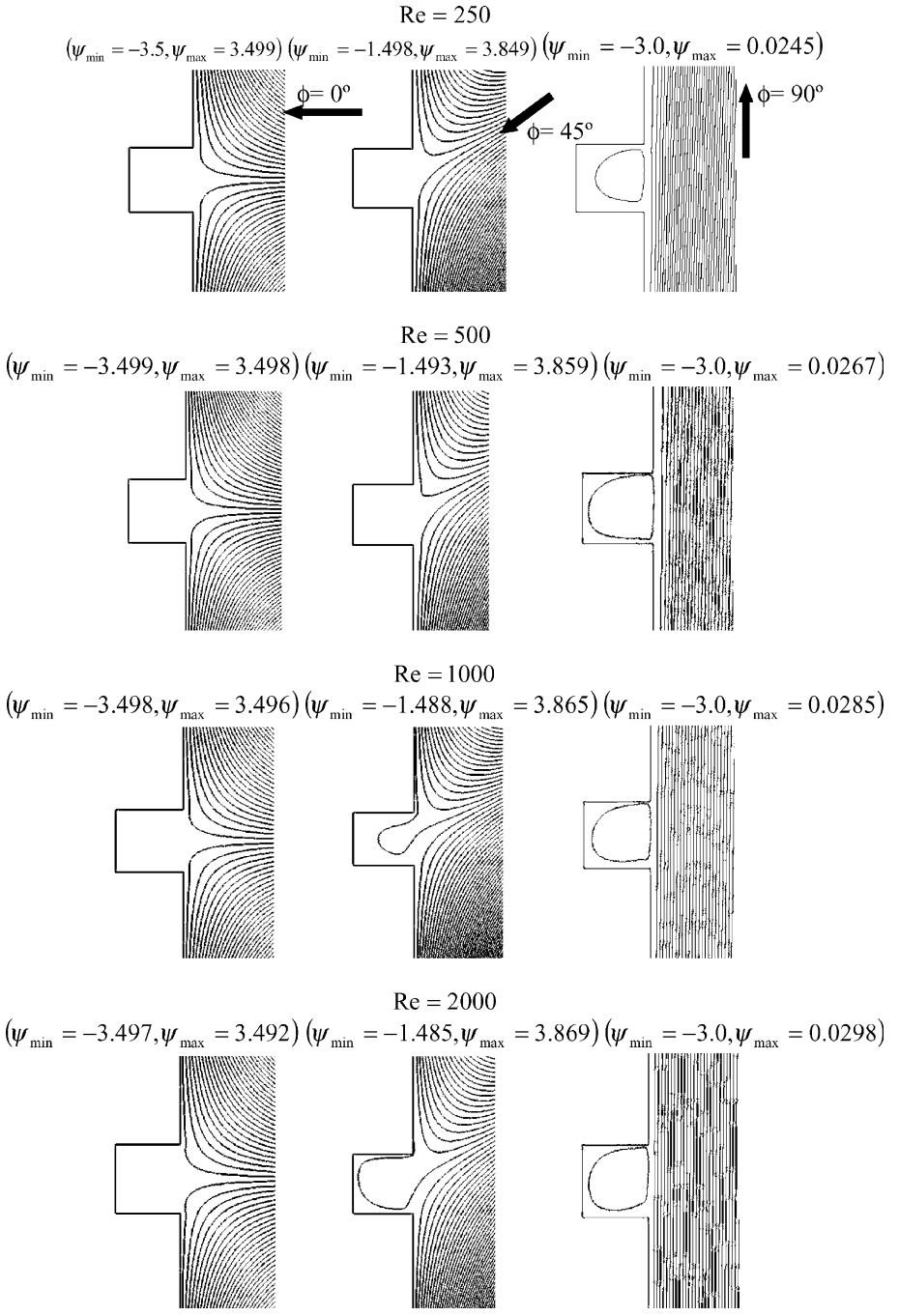

Fig. 6. The effect of the Reynolds number on the streamlines for different flow configurations (AR = 1, $Gr = 100$).

exists along the extended vertical wall from the cavity and consequently, the overall plume temperature decreases. Further increase in the Reynolds number ($Re \geqslant 2000$), causes the streamlines to have a symmetrical behavior about the horizontal centerline of the cavity.

The influence of the variation of the Reynolds number on the streamlines and the isotherms for high Grashof number at 45° flow angle of attack is demonstrated in Fig. 9. It is seen in this figure that the flow pattern within the enclosure remains unaltered for high Reynolds number due to the substantial influence from

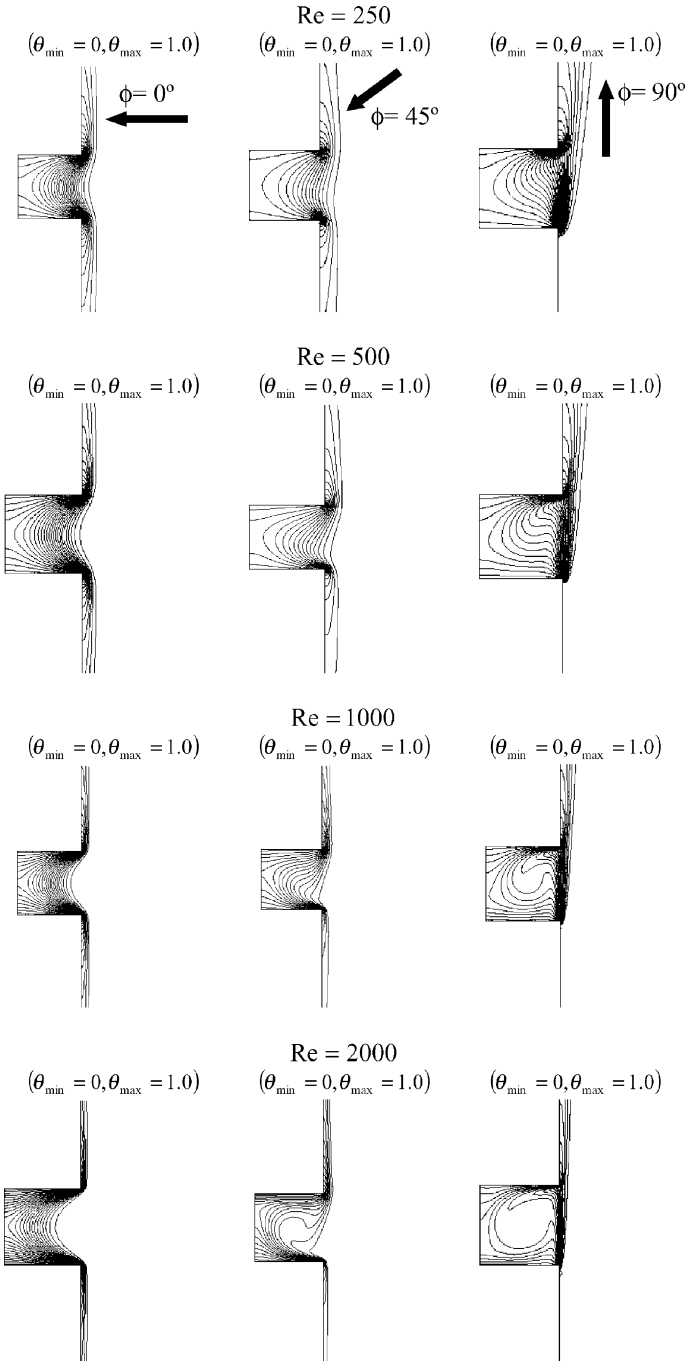

Fig. 7. The effect of the Reynolds number on the isotherms for different flow configurations (AR = 1, $Gr = 100$).

the external flow. This situation is different with respect to the isotherm pattern. As the Reynolds number increases, the influence of the forced convection within the cavity increases resulting in a thinner thermal boundary layer along both the lower and upper horizontal walls of the cavity. For $Re = 5000$, the core of the cavity is maintained at the same temperature as the external flow temperature.

For vertical external flow, Fig. 10 illustrates the effect of varying Reynolds number on the streamlines and the isotherms within the enclosure for $Gr = 10^5$. For small Reynolds number, the effect of the external forced flow

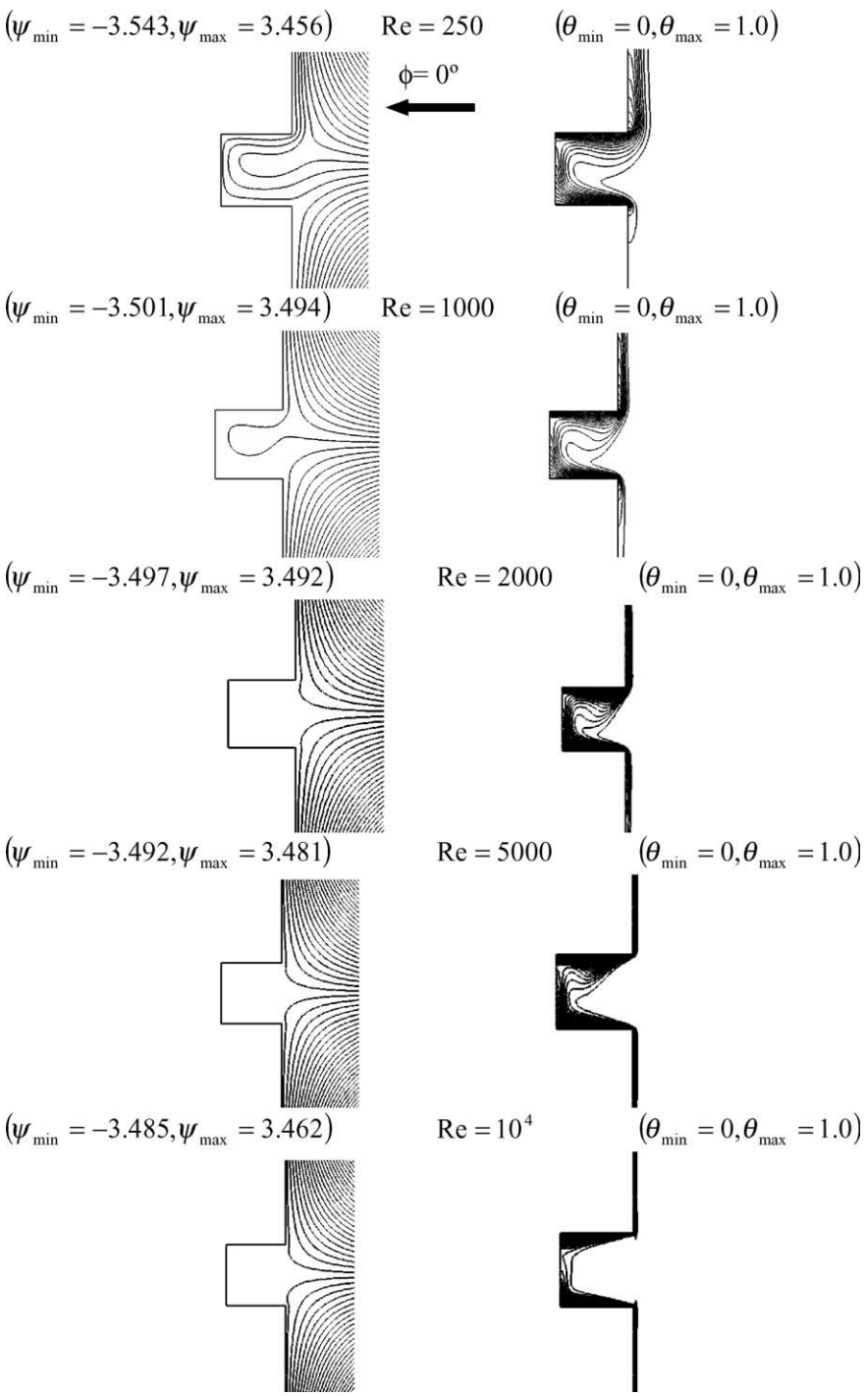

Fig. 8. The effect of Reynolds number on the streamlines and the isotherms (AR = 1, $Gr = 10^5$, angle = 0°).

is overwhelmed by the effect of natural convection inside the cavity. As such, the cold flow is sucked inside the cavity where it gets warm along the lower horizontal wall. This is due to a large suction pressure within the enclosure compared to the external flow pressure. For $Re \geqslant 3000$, the isotherms are clustered at the aperture plane and the streamlines patterns are almost unchanged due to the dominant effect of the external flow in which

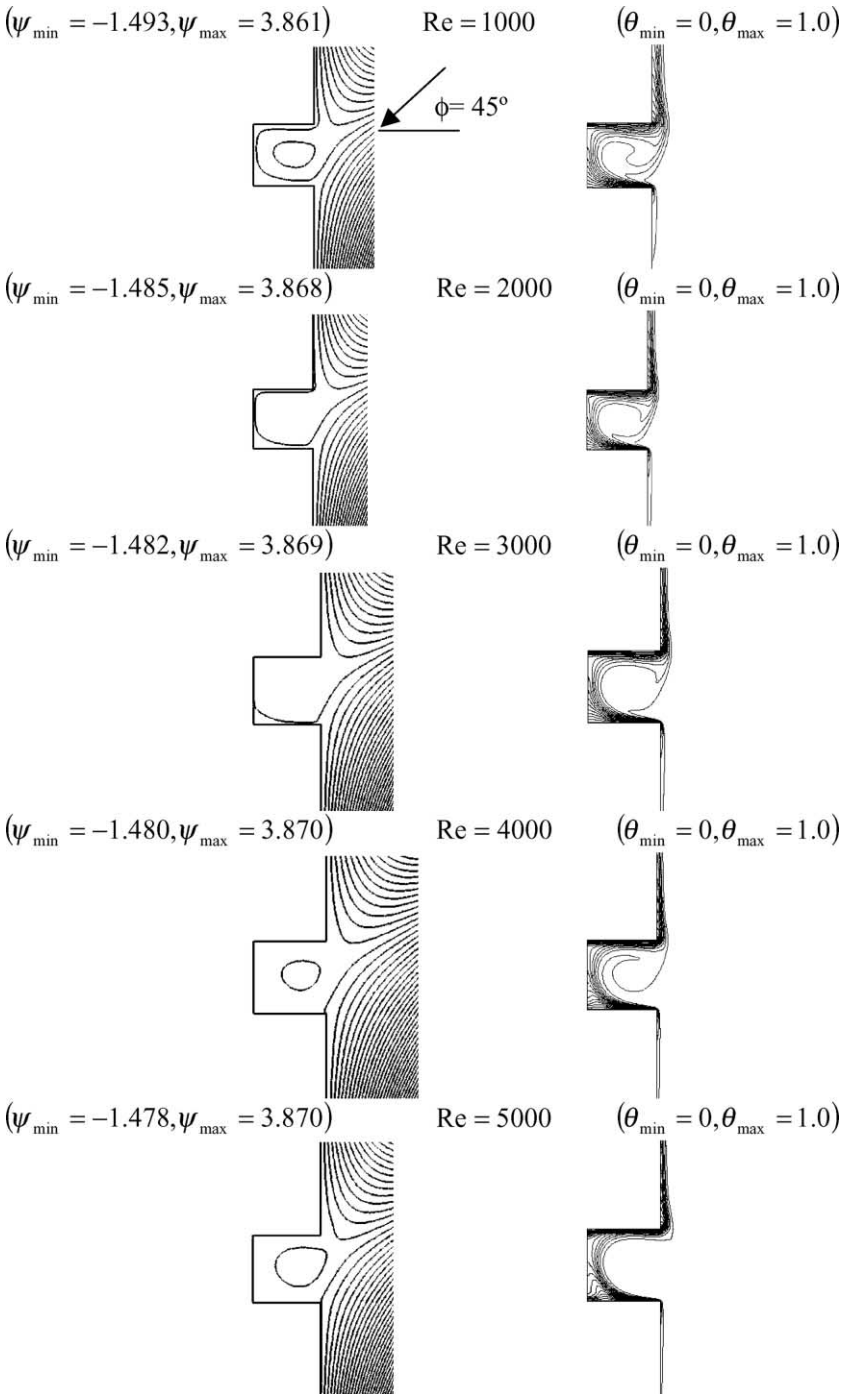

Fig. 9. Effect of Reynolds number on the streamlines and the isotherms (AR = 1, $Gr = 10^5$, angle = 45°).

the flow does not penetrate much into the cavity. As such the external flow pressure balances the suction pressure within the enclosure.

The effect of varying the aspect ratio on the streamlines and the isotherms for $Gr = 10^5$ and $Re = 100$ is shown in Figs. 11 and 12. Fig. 11 shows that as the aspect ratio increases the speed of the incoming fluid decreases and the hydrodynamic boundary layer thickness keeps on decreasing along the upper and lower horizontal walls of the cavity. The isotherms in

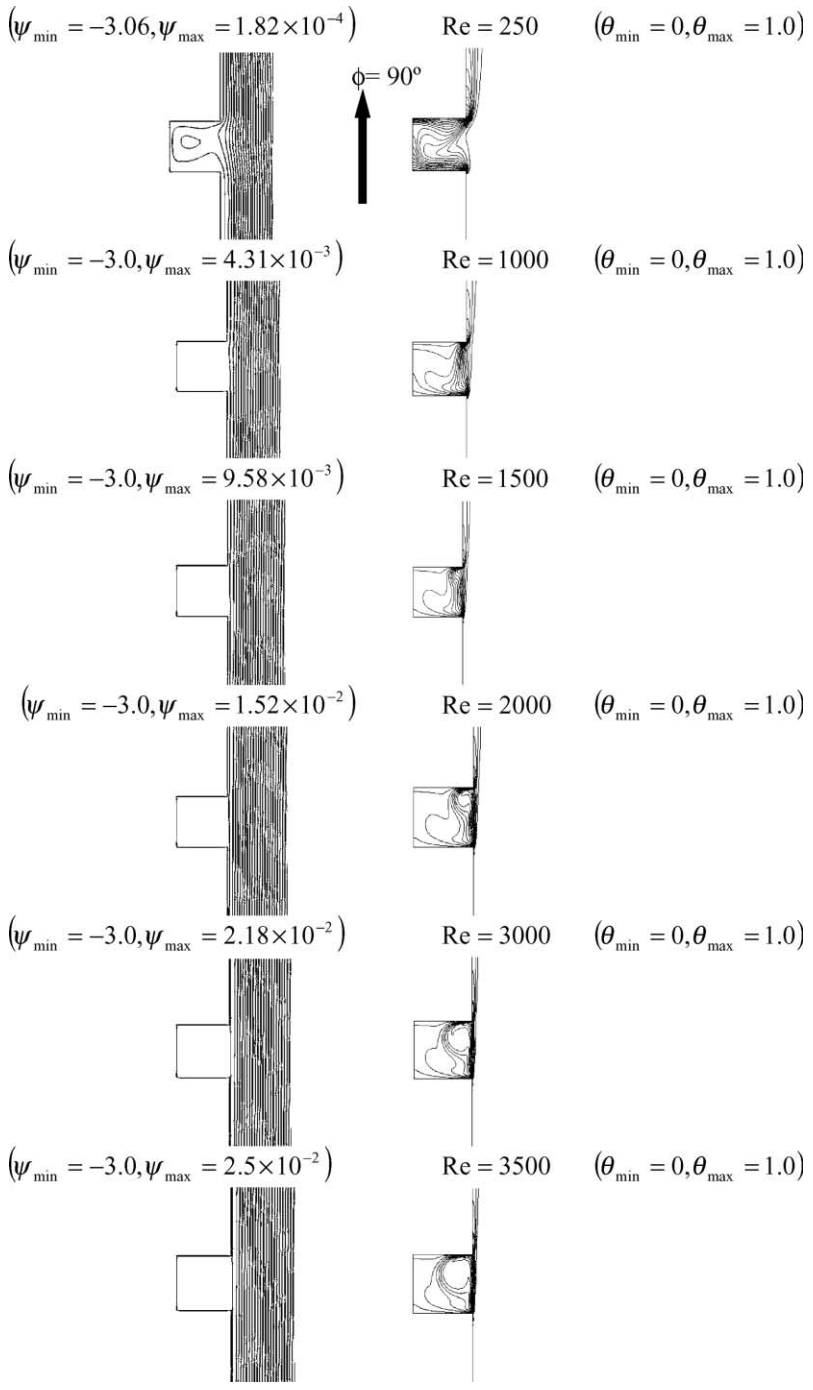

Fig. 10. Effect of Reynolds number on the streamlines and the isotherms (AR = 1, $Gr = 10^5$, angle = 90°).

Fig. 12 shows that as the aspect ratio decreases, the incoming fluid velocity increases resulting in a heat transfer enhancement from both horizontal walls due to a thinner thermal boundary layer. Fig. 12 illustrates that a thermally stratified region along the extended vertical wall becomes more established with higher aspect ratios.

The effect of the Reynolds number on the temperature and the velocity profiles along the aperture plane for zero flow angle of attack and Grashof numbers of

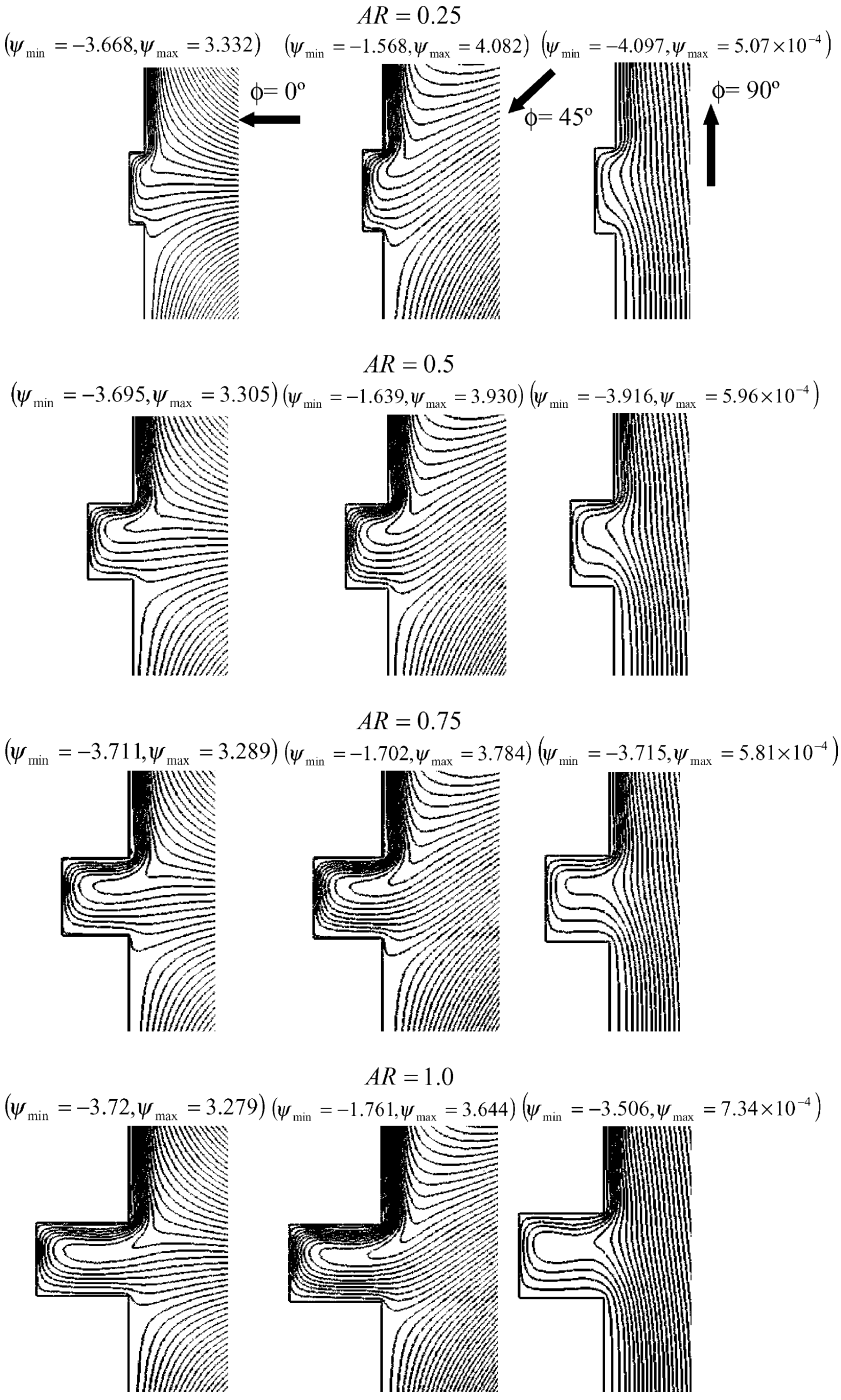

Fig. 11. The effect of varying the aspect ratio on the streamlines for three different flow configurations ($Gr = 10^5$, $Re = 100$).

10^2 and 10^5 is shown in Fig. 13. An interesting result is illustrated in this figure in which the temperature profiles reach the surrounding temperature for high Reynolds number except for regions close to the horizontal walls of the cavity. As such a thermal protection of the cavity from the external medium is perfectly assured. This effect is more pronounced at low Richardson numbers ($Ri = Gr/Re^2$). Moreover, Fig. 13 shows that the horizontal velocity component is almost zero at the aperture plane except at a region closer to the upper horizontal

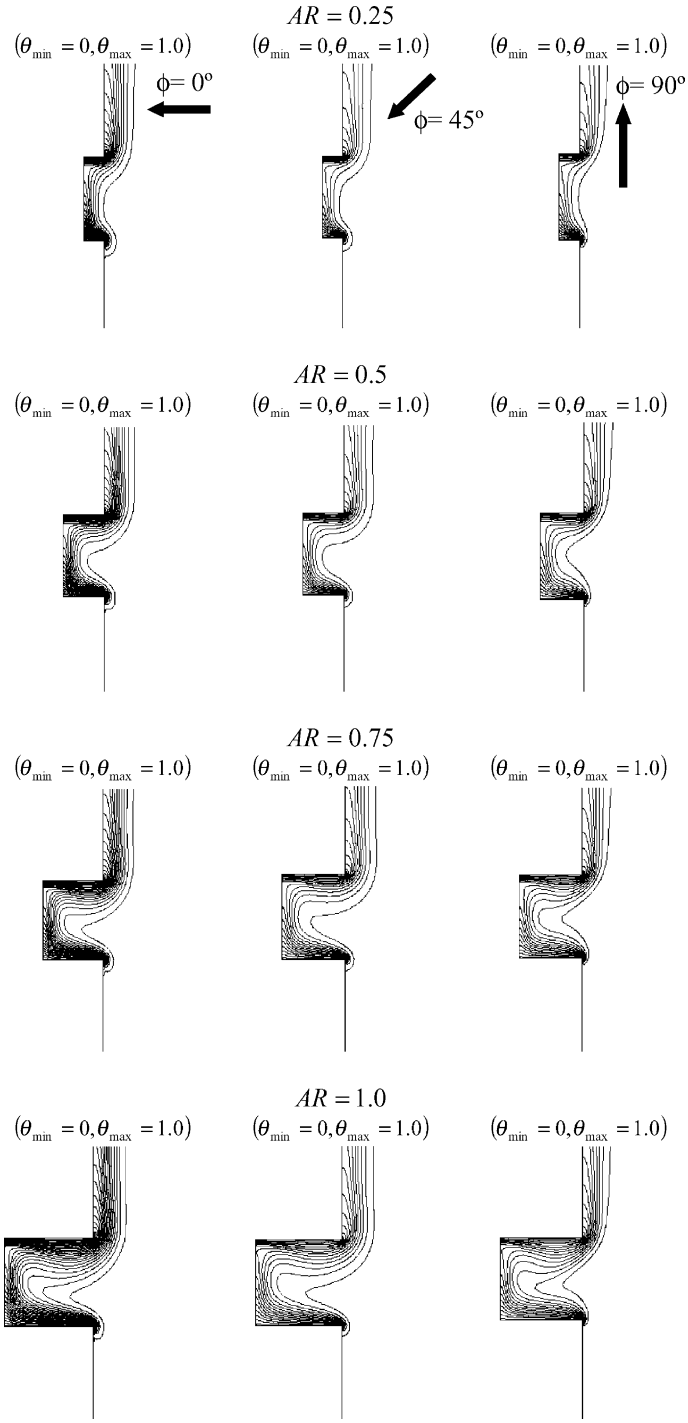

Fig. 12. The effect of varying the aspect ratio on the isotherms for different flow configurations ($Gr = 10^5$, $Re = 100$).

wall of the enclosure where the effect of the external flow is appreciated.

For 45° angle of attack, Fig. 14 shows the variation of the temperature and the velocity profiles at various Reynolds numbers for low and high Grashof numbers. The horizontal velocity component illustrates that as the Reynolds number increases the hydrodynamic boundary layer is well established along the horizontal surfaces as

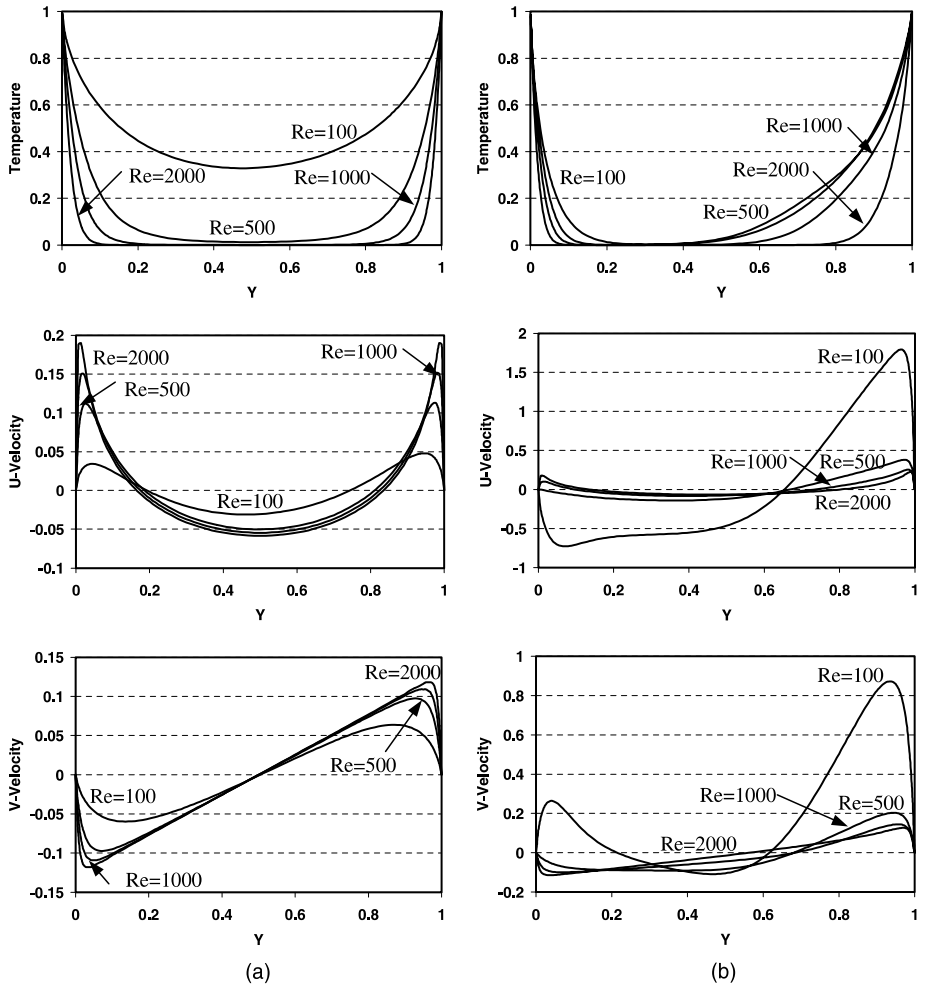

Fig. 13. Temperature and velocity profiles at the aperture plane for zero flow angle of attack (a) AR = 1, $Gr = 100$, (b) AR = 1, $Gr = 10^5$.

a result of the induced flow. As such the velocity gradients are steeper at the lower surface of the enclosure as compared to the upper surface.

The effect of varying Reynolds number on the temperature and the velocity profiles of 90° flow angle of attack configuration is shown in Fig. 15 for low and high Grashof numbers. For low Grashof number, the temperature profiles show steeper temperature gradients at the upper wall than the lower wall indicating more heat transfer from that surface. The horizontal velocity component profiles demonstrate that the velocity is almost zero for all Reynolds numbers except at the top right corner of the cavity where the velocity is appreciated. Therefore, the external flow does not penetrate much into the cavity except at the upper part of the cavity. For higher Grashof number ($Gr = 10^5$), there is a rapid increase in the exit velocity for low Reynolds number ($Re = 100$). This is due to the combined effect of the external flow along with the ejection mechanism, which causes the fluid to leave the cavity at higher speeds. As the Reynolds number increases, the peak velocity values decrease dramatically due to the predominant effect of the external flow. As such, the suction and ejection mechanisms established by natural convection within the cavity become less prominent, thus reducing the fluid penetration into the cavity.

The effect of the Reynolds number on the average Nusselt number for different flow configurations is shown in Fig. 16 for low and high Grashof numbers. For $Gr = 100$, Fig. 16a illustrates that 45° flow has the highest average Nusselt number along the lower surface of the cavity compared to other configurations. This can be attributed to the direct jet impingement on the lower surface, which causes better heat transfer. However, 90° flow experiences the lowest average Nusselt number along the lower surface since the isotherms along that

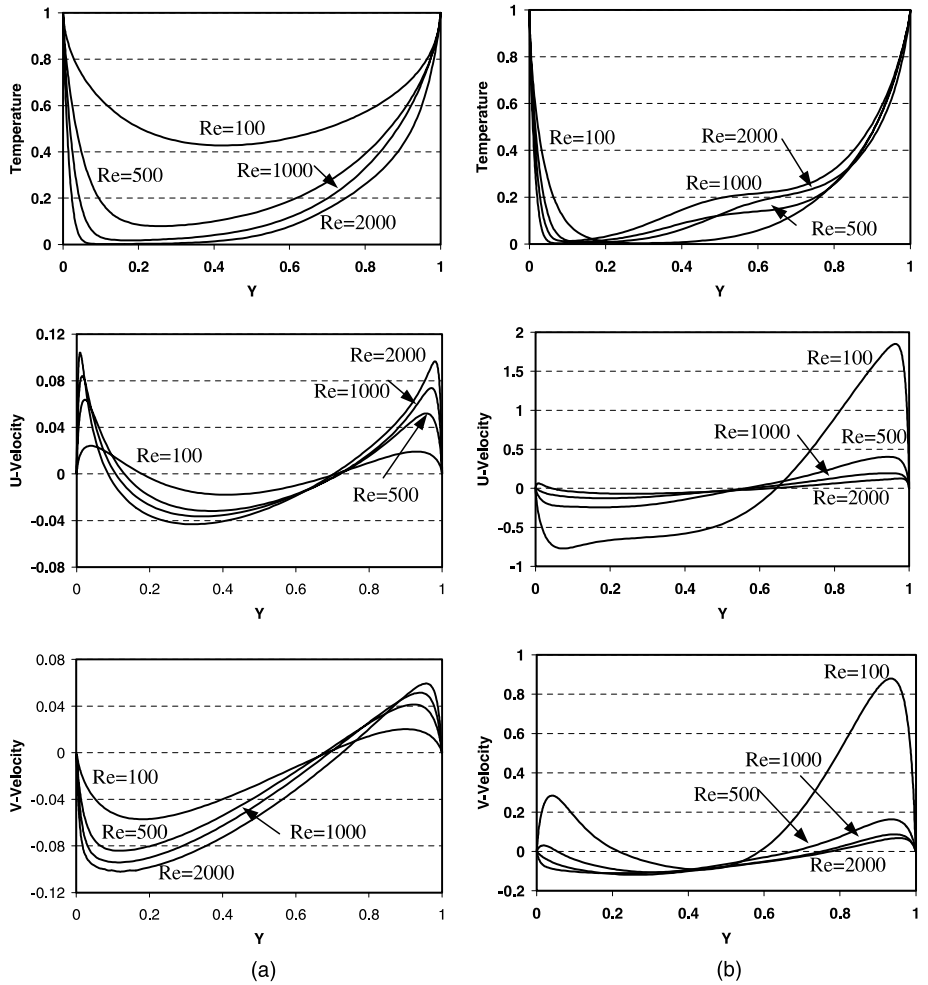

Fig. 14. Temperature and velocity profiles at the aperture plane for 45° flow angle of attack (a) AR = 1, $Gr = 100$, (b) AR = 1, $Gr = 10^5$.

surface are almost thermally stratified which reveals that most of the heat transfer from that surface is carried out by conduction. This picture is reversed for the upper Nusselt number where 90° flow angle of attack has the highest average Nusselt number.

As the Grashof number increases to $Gr = 10^5$ (Fig. 16b), an interesting situation is observed for the 90° flow angle of attack. It is seen in this figure that the lower Nusselt number decreases as the Reynolds number increases and then remains almost constant for Reynolds number greater than 1500. This is because the flow does not penetrate much into the cavity except at the upper surface of the cavity. Also, for higher Reynolds numbers, the flow patterns are completely controlled by the external flow rather than the natural convection. This is confirmed in Fig. 10. However, for $Re < 1000$, the external flow is overwhelmed by the natural convection inside the cavity resulting in well established thermal boundary layers along the upper and lower surfaces of the cavity. For $Re \geqslant 1000$, the thermal boundary layer thickness increases along the lower surface of the enclosure resulting in lower heat transfer and consequently lower average Nusselt number (see for instance Fig. 10).

For the upper average Nusselt number, Fig. 16b shows that 45° flow is the highest compared to the other configurations. It is worth noting that the upper average Nusselt number for the 90° flow angle of attack configuration first decreases as the Reynolds number increases and then increases for $Re \geqslant 1000$. For low Reynolds numbers, free convection contribution is dominant resulting in well established thermal boundary layers. As the Reynolds number increases, the thermal boundary layer thicknesses increases along both surfaces resulting in lower heat transfer. A critical Reynolds number ($Re \cong 900$) exists, where the external flow contribution becomes dominant as compared to the natural

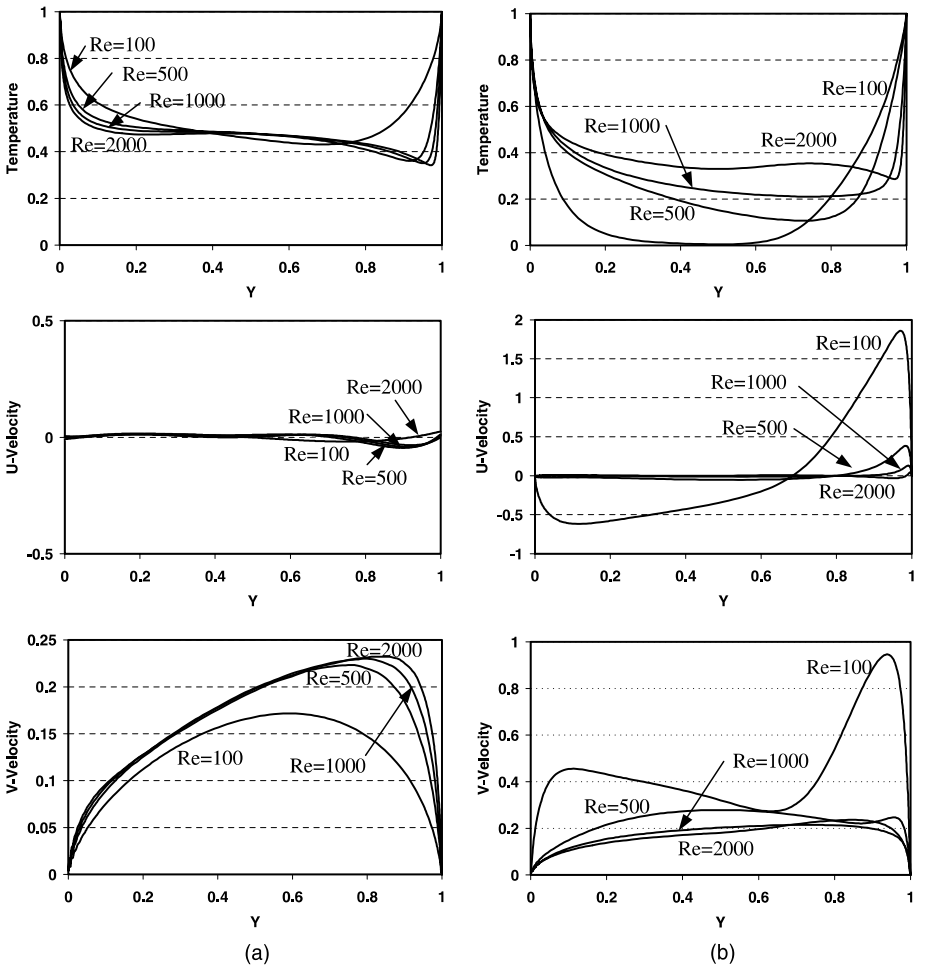

Fig. 15. Temperature and velocity profiles at the aperture plane for 90° flow angle of attack (a) AR = 1, $Gr = 100$, (b) AR = 1, $Gr = 10^5$.

convection effects. This point can be seen in the collective contribution displayed in Fig. 10.

4. Heat transfer correlations

The average Nusselt numbers along the upper and lower walls of the cavity for the three basic configurations are correlated in terms of $100 \leqslant Re \leqslant 5000$, $0.25 \leqslant \mathrm{AR} \leqslant 1$, and $10^2 \leqslant Gr \leqslant 10^5$.

These correlations can be expressed as follows:

$10^2 \leqslant Re \leqslant 10^3$:

$$\begin{aligned} Nu_i = {} & 4.52148 + 1.2685 \times 10^{-4}\, Gr - 1.03813 \times 10^{-9}\, Gr^2 \\ & + 1.75359 \times 10^{-15}\, Gr^3 - 8.2623 \times 10^{-34}\, Gr^6 \\ & - 3.69155\,\mathrm{AR} - 8.3706 \times 10^{-25} (Gr\,Re)^3 \\ & + 3.64 \times 10^{-3} (\mathrm{AR}\, Re) + 0.02871 \cos\theta \\ & - 3.59 \times 10^{-6} (\cos\theta)^3 - 8.7661 \times 10^{-8} (\cos\theta\, Gr) \\ & - 3.248 \times 10^{-5} (\cos\theta\, Re) \end{aligned} \tag{6}$$

$10^3 \leqslant Re \leqslant 5 \times 10^3$:

$$\begin{aligned} Nu_i = {} & 17.92963 - 7.26054 \times 10^{-8} Re^2 - 16.06846\,\mathrm{AR} \\ & + 3.7263 \times 10^{-15} (\mathrm{AR}\, Gr)^3 + 1.77 \times 10^{-2} (\mathrm{AR}\, Re) \\ & + 0.11552 \cos\theta - 1.738 \times 10^{-5} (\cos\theta)^3 \\ & - 3.63294 \times 10^{-7} (\cos\theta\, Gr) - 6.15 \times 10^{-6} (\cos\theta\, Re) \end{aligned} \tag{7}$$

$10^2 \leqslant Re \leqslant 10^3$:

$$\begin{aligned} Nu_o = {} & 7.91132 + 7.546 \times 10^{-5}\, Gr - 1.9892 \times 10^{-34}\, Gr^6 \\ & + 0.00221 Re - 14.82577\,\mathrm{AR} + 7.90395\,\mathrm{AR}^2 \\ & - 3.05132 \times 10^{-8} (Gr\, Re) - 2.9292 \\ & \times 10^{-10} (\mathrm{AR}\, Gr)^2 + 4.44977 \times 10^{-16} (\mathrm{AR}\, Gr)^3 \\ & - 1.82544 \times 10^{-7} (\cos\theta\, Gr) \end{aligned} \tag{8}$$

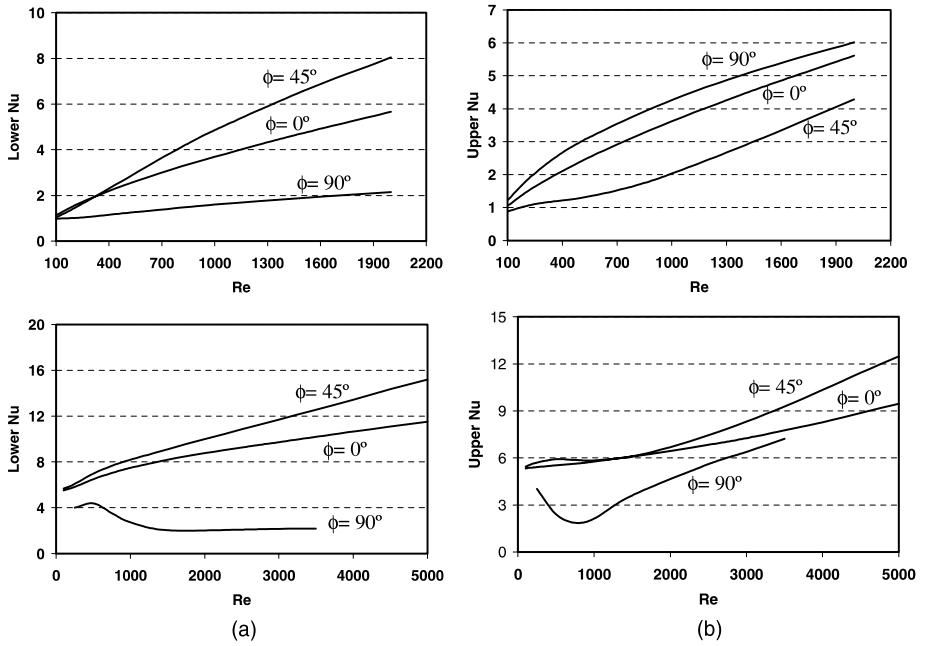

Fig. 16. The effect of the Reynolds number on the average Nusselt number for three different flow angles of attack: (a) AR = 1, $Gr = 10^2$, (b) AR = 1, $Gr = 10^5$.

$10^3 \leqslant Re \leqslant 5 \times 10^3$:

$$Nu_o = 18.95393 + 1.81749 \times 10^{-20}\, Gr^4 - 28.16662\,\mathrm{AR} + 13.55405\,\mathrm{AR}^2 + 1.78451 \times 10^{-17}(Gr\,Re)^2 - 8.0366 \times 10^{-12}(\mathrm{AR}\,Re)^3 - 2.93382 \times 10^{-7}(\cos\theta\, Gr) + 2.166 \times 10^{-5}(\cos\theta\,\mathrm{Re}) - 0.0328(\cos\theta\,\mathrm{AR}) \quad (9)$$

5. Conclusions

Mixed convection heat transfer in an open-ended enclosure is analyzed numerically in this work for three basic configurations. Effects of a wide range of pertinent parameters such Grashof number, Reynolds number, and the aspect ratio are investigated in the present study. The present results show that the lower and the upper average Nusselt numbers increase almost linearly with the Reynolds numbers for the three configurations at low Grashof number. In addition, for low Grashof number, the results show that the lower average Nusselt number is the highest for the 45° flow angle of attack and is the lowest for the 90° flow angle of attack. However, the upper Nusselt number is found to be the highest for the 90° flow angle of attack and is the lowest for the 45° flow angle of attack. For high Grashof number, the results show that the lower and the upper average Nusselt numbers are the highest for the 45° flow angle of attack and are the lowest for the 90° flow angle of attack at various Reynolds numbers. An interesting result is observed in this investigation, which illustrates that the horizontal flow can be used to insulate the cavity from the surrounding medium thus minimizing the heat exchange between the cavity and the surroundings. Also, the existence of a critical Reynolds number for 90° flow angle of attack is established and discussed.

Acknowledgements

The grant from National Sciences and Engineering Research Council of Canada (NSERC-2002) is acknowledged and appreciated.

References

[1] C. Desai, K. Vafai, Three-dimensional buoyancy-induced flow and heat transfer around the wheel outboard of an aircraft, Int. J. Heat Fluid Flow 13 (1992) 50–64.
[2] F. Penot, Numerical calculation of two-dimensional natural convection in isothermal open cavities, Numer. Heat Transfer 5 (1982) 421–437.
[3] O. LeQuere, J.A.C. Humphery, F.S. Sherman, Numerical calculation of thermally driven two-dimensional unsteady laminar flow in cavities of rectangular cross section, Numer. Heat Transfer 4 (1981) 249–283.

[4] Y.L. Chan, C.L. Tien, A numerical study of two-dimensional natural convection in square open cavities, Numer. Heat Transfer 8 (1985) 65–80.
[5] Y.L. Chan, C.L. Tien, A numerical study of two-dimensional laminar natural convection in shallow open cavities, Int. J. Heat Mass Transfer 28 (1985) 603–612.
[6] M.L. Doria, A numerical model for the prediction of two-dimensional unsteady flows of multi-component gases with strong buoyancy effects and recirculation, Notre Dame Report, TR-37191-74-4, 1974.
[7] H.R. Jacobs, W.E. Mason, W.T. Hikida, Natural convection in open rectangular cavities, in: Proc. Fifth Int. Heat Transfer Conf., Tokyo, Japan, vol. 3, 1974, pp. 90–94.
[8] H.R. Jacobs, W.E. Mason, Natural convection in open rectangular cavities with adiabatic sidewalls, in: Proc. 1976 Heat Transfer and Fluid Mech. Inst., Stanford University Press, Stanford, 1976, pp. 33–46.
[9] K.S. Chen, J.A.C. Humphery, F.S. Sherman, Experimental investigation of thermally driven flow in open cavities of rectangular cross-section, Phil. Trans. R. Soc. London A 316 (1985) 57–84.
[10] V. Serans, I. Kyriakides, Natural convection in an open cavity, in: Proc. Seventh Int. Heat Transfer Conf., Munchen, Germany, vol. 2, 1982, pp. 275–286.
[11] R.A. Showole, J.D. Tarasuk, Experimental and numerical studies of natural convection with flow separation in upward-facing inclined open cavities, J. Heat Transfer 115 (1993) 592–605.
[12] M.M. Elsayed, W. Chakroun, Effects of aperture geometry on heat transfer in tilted partially open cavities, J. Heat Transfer 121 (1999) 819–827.
[13] K. Vafai, J. Ettefagh, The effects of sharp corners on buoyancy-driven flows with particular emphasis on outer boundaries, Int. J. Heat Mass Transfer 33 (1990) 2311–2328.
[14] K. Vafai, J. Ettefagh, Thermal and fluid flow instabilities in buoyancy-driven flows in open-ended cavities, Int. J. Heat Mass Transfer 33 (1990) 2329–2344.
[15] H. Mhiri, S. El Golli, A. Berthon, G. Le Palec, P. Bournot, Numerical study of the thermal and aerodynamic insulation of a cavity with a vertical downstream air jet, Int. Commun. Heat Mass Transfer 25 (1998) 919–928.
[16] S. Besbes, H. Mhiri, S. El Golli, G. Le Palec, P. Bournot, Numerical study of a heated cavity insulated by a horizontal laminar jet, Energy Convers. Manage. 42 (2001) 1417–1435.
[17] K. Khanafer, K. Vafai, Buoyancy-driven flows and heat transfer in open-ended enclosures: elimination of the extended boundaries, Int. J. Heat Mass Transfer 43 (2000) 4087–4100.
[18] K. Khanafer, K. Vafai, Effective boundary conditions for buoyancy-driven flows and heat transfer in fully open-ended two-dimensional enclosures, Int. J. Heat Mass Transfer 45 (2002) 2527–2538.
[19] FIDAP Theoretical Manual, Fluid Dynamics International, Evanston, IL, 1990.